DETECTING ACCELEROMETRIC NONLINEARITIES IN THE INTERNATIONAL SPACE STATION

N. Sáez[a], Jna. Gavaldà[a, *], X. Ruiz[a,b], V. Shevtsova[c]

[a] Departament de Química Física I Inorgànica, Universitat Rovira I Virgili, 43007 Tarragona, Spain.
[b] Institut d'Estudis Espacials de Catalunya, IEEC,43002 Barcelona, Spain.
[c] Department of Chemical Physics, MRC, Université Libre Bruxelles, Brussels, Belgium.

ABSTRACT

The present work aims to study mechanical nonlinearities detected in the accelerometric records during a thermodiffusion experiment performed at the International Space Station, ISS. In that experiment the test cell was subjected to harmonic vibrations of different frequencies and amplitudes. Accelerometric data associated to the runs were downloaded from NASA PIMS website. Second order spectral analysis shows that the shaker modifies the normality of the data and introduces nonlinearities in the distribution of energy. High Order Spectral Analysis, HOSA, based on the bispectrum, bicoherence, trispectrum and tricoherence functions enabled us to study the kind of these nonlinearities. Additionally, a new method using the biphase and triphase histograms help us to assess if quadratic and/or cubic phase coupling mechanisms are the responsible of the anomalous nonlinear energy transfer detected. Finally, the RMS acceleration values are investigated to check if the vibratory limit requirements of the ISS are exceeded. This methodology is important not only in generic research of aerospace engineering but also in space sciences in order to help space researchers to characterize more globally their experiments. Mention finally that HOSA techniques are not new, but never have been used in the analysis of accelerometric data coming from the ISS.

1. Introduction

Digital signal processing is the only suitable tool to vibrationally characterize motorized experiments as the so-called "Influence of VIbrations on DIffusion of Liquids, IVIDIL" one. The global scientific objective of this experiment was to investigate the impact of harmonic vibrations of different amplitudes and frequencies on the study of diffusion and thermodiffusion processes. IVIDIL, located into the Columbus module of the International Space Station, was operative since September 2009 until January 2010 successfully carrying out about fifty different runs at different initial conditions [1, 2]. The objective of the present work is also related with this experiment but restricted only to the study of its different vibrational aspects.

To characterize vibrations in time domain first and second order statistics use the mean and the variance. In the frequency domain the power spectrum helps to complete the description [3]. But, second order statistical techniques are only sufficient for describing linear processes and a vibrating mechanical system often shows unstable, nonGaussian and nonlinear characteristics to some extent, especially when the mechanical system become defective. Mechanical failures, if any, are always preceded with changes from linear to strong nonlinear dynamics, so it is difficult for conventional analyses based on the Fourier transform to detect faults. High Order Spectral Analyses, HOSA, must then be used in order to provide a more effective tool to extract information due to deviations from Gaussianity, to recover the true phase character of the signals and to detect and quantify nonlinearities in the corresponding time series [4-6]. More specifically, higher order spectral techniques have successfully been used to detect fatigue cracks [7-9] as well as faults in ball bearings and gears [10, 11] and in the monitoring of rotating machines [12-14]. At this respect higher order spectral techniques have also been applied to complete the Motor Current Signature Analysis, MCSA, one of the most spread procedures for health monitoring of the motor since decades [15]. Mention also that higher order techniques have successfully been applied for machine condition monitoring in the cases of low signal-to-noise rate or when the spectral band of the signal to be processed was overlapped by spectral components of an interference signal making impossible to identify which signal the spectral component belongs to [16]. Global accelerometric nonlinearities, related with structural dynamics, have also been detected in modal correlation analyses performed for different configurations of the station [17, 18] but these kind of analyses are far from the purpose of the present work.

[*] Corresponding author. Tel.: +34 977 55 95 18; fax: +34 977 55 95 63.
E-mail address: fina.gavalda@urv.cat (Jna. Gavaldà)

In previous works [19, 20] we analyzed data coming from two and three accelerometric sensors when the shaking motor unit of the above-mentioned IVIDIL experiment was active or inactive. Now, in this work, we focus our attention on a different situation considering data coming only from a single sensor during active periods of the shaker in which the translational oscillatory movement has different frequencies and amplitudes. In particular, the present signals cover complete experiments -roughly 18 hours- with shaking frequencies of 2 and 2.8 Hz respectively. Amplitudes are, in all cases, between 15 and 62 mm. It should be pointed out that despite the active sensor is situated in this rack is near, but not on the experiment.

Based on the above-mentioned accelerometric signals and using standard second order and higher order spectral techniques the aim of the present work is to carry out a deep comparative analysis in order to characterize the distortions generated by the activity of the mechanical system, in particular, by the different frequencies and amplitudes of the oscillatory movements applied. To do so we will emphasize on polispectral techniques based on the calculation of bispectrum and trispectrum functions. Bispectrum function -third order spectrum- is related with the skewness of the signal, so it can detect asymmetric nonlinearities. In the same way the trispectrum -fourth order spectrum- is sensitive to the signal kurtosis, therefore it can detect symmetric nonlinearities. Bispectrum, trispectrum and their normalized functions, bicoherence and tricoherence, will enable us to study here what kind of nonlinearity is active all along the experiment [21-23].

It is important to note that malfunctions in motorized experiments, if any, are not easy to be removed in space platforms, so their detection and characterization is very important because the signal nonlinearities generated by these malfunctions can even change the nominal conditions of the experiment confusing the experimenter and generating doubtful results. This simple, but powerful, reason enhances the relevance of the present work not only in generic studies of mechanical systems but also in space studies.

2. Mathematical background

All signals used here come from the same SAMSes08 (Space Acceleration Measurement System) accelerometer with a sampling rate of 500 Hz, a cutoff frequency of 200 Hz and a gain of 8.5. Signals have freely been downloaded thanks to NASA Principal Investigator Microgravity Services, PIMS, website[†] as binary files. Data units are in g and in order to eliminate possible instrument bias we have systematically demeaned all the raw signals before attempt any mathematical manipulation. The position and location / orientation of the SAMS sensor against the International Space Station absolute coordinate system (SSA: X_A, Y_A, Z_A) is detailed in the bibliography [24]. It should be pointed out that all results presented mainly refer to the X_A direction because this coincides with the shaking one.

Frequency domain analyses are based on the Power Spectral Density, PSD, estimated by the Welch method. As it is well known, this method splits the signal into overlapping segments, thirty three in the present case, calculates the periodogram of each one of them using Hanning windows and averages the results to produce the final power spectral density result [25]. If the distribution associated to a signal is not normal, HOSA techniques must be used. The Fourier Transform, FT, of the third order cumulant, called the bispectrum (Eq. (1)) has been estimated as a direct average of the triple products of Fourier Transforms over K segments (direct method) [26]:

$$\hat{S}_{3x}(f_1, f_2) = E[X(f_1)X(f_2)X^*(f_1 + f_2)] \tag{1}$$

where X denotes the Fourier Transform of segment k and X* its complex conjugate. Notice that the bispectrum, as a generic complex magnitude, has module and phase. For each one of the different K segments, the module and biphase can be written as:

$$\left|S_{3x,k}(f_1, f_2)\right| = |X(f_1)X(f_2)X^*(f_1 + f_2)| \tag{2}$$

$$\angle S_{3x,k}(f_1, f_2) = \theta(f_1) + \theta(f_2) - \theta(f_1 + f_2) \tag{3}$$

where θ represents the phase of the FT at two different generic frequencies f_1, f_2.

In the present case, Fourier Transforms have been calculated considering 2048 FT points in each one of the 14000 non overlapped segments in which the signal was initially divided. Hanning windows have been used in each segment. Symmetry relations in the frequency plane (f_1, f_2) resulting from the definition of the discrete bispectrum, makes that the first quadrant of this plane contains two regions symmetric respect the straight line $f_1 = f_2$ [27].

Peaks of the bispectrum where the components are coupled in frequency and phase can be correlated with a Quadratic Phase Coupling, QPC, phenomenon. Only quadratic phase coupling gives evidence of quadratic nonlinearities in the system under study. Frequency coupling between two frequency components of a signal results in a contribution at a frequency equal to their sum. Phase coupling exists when the phase of bispectrum is zero. However, this last condition is a delicate one because it implies the consideration of the phases of the Fourier Transforms at two frequencies as well as at its sum (see Eq. 3). In effect, Fig.1 shows a typical phase variation as a function of the frequency. In the present case it is clear that around some

[†] http://pims.grc.nasa.gov/html/ISSAccelerationArchive.html

relevant frequencies the value of the phases is strongly dependent on the frequency value considered. A small variation quickly transforms zero into +π or -π rad. Due to the limitations inherent to discrete calculations involving the sampling frequency and the number of points of the FT used and taking into account the also discrete -equivalently, not exact- information of the position of the different bispectrum peaks it is extremely difficult to obtain exact phase values. In other words, it is very easy to have highly scattered values of the phase masking any kind of reasonable explanation. To properly consider the above-mentioned effects concerning the phase values, in the present work we have considered as equivalents the values of 0 and ±π rad. This equivalence is automatically translated to the present quadratic phase coupling condition in the sense that the phase of the bispectrum, the biphase, could now be equivalently zero or ±π rad if phase coupling is detected. In addition, due to the above-mentioned signal splitting, each one of the different segments in which the signal has been divided generate a subset of phase results which finally be synthesized using a global biphase histogram.

As an example, Fig. 2 shows typical IVIDIL biphase results during experiments with vibrations. Cases "a)" and "d)" of Fig. 2 correspond to a QPC typical situation because the biphase is distributed around zero (Fig. 2a) or ±π (Fig. 2d). The literature [28] also indicates that peaks in the bispectrum can also be associated with a constant phase, CP, situation. In these cases the system is coupled in frequency but not in phase. The biphase is constant but nonzero. Fig. 2c and Fig. 2f typically illustrates this behavior. But, with this new tool we have detected the existence of a third case, labeled PQPC, partial quadratic phase coupling, when only a percentage of biphase values is centered in zero or ±π rad (Fig. 2b and 2e). In this last case the consideration of the histogram shape enabled us the calculation of a quantitative percentage of quadratic phase coupling based on the distribution of the maxima in the corresponding histogram. To do so we have considered an acceptance region around each maximum of interest counting all the values inside this region. If the biphase values are approximately normal distributed around the peak, the use of a significance level of 0.95 determines the width of this region [29-31]. In the present study an acceptance region of ±0.1 rad has typically been applied in practically all the cases. On the other hand, to ensure statistical confidence, the maximum segment size to compute the FT (here 2048 FT points) should be the $(r-1)^{th}$ root of the total length of the data when handling the r^{th} order spectrum [26, 32]. In the case of the present bispectrum calculations there is no problem at all for accomplishing this condition.

The bispectrum is usually normalized in such a way that it gives a new measure, the bicoherence function, with approximately flat variance across all bifrequencies (f_1, f_2) [33],

$$\widehat{\mathrm{bic}}^2_{3\mathrm{x}}(f_1, f_2) = \frac{|\hat{\mathrm{S}}_{3x}(f_1,f_2)|^2}{E[|X(f_1)X(f_2)|^2]\ \mathrm{E}[|\mathrm{X}(f_1+f_2)|^2]} \tag{4}$$

The quantitative determination of the bicoherence is a delicate question because the low values of the factors in the denominator could generate a fictitious peak distribution which needs to be carefully corrected using different strategies [29, 34, 35]. In our case we adopted the common threshold methodology, that is to say, when the magnitudes that appears in the bicoherence do not overcome a determined threshold, the bicoherence is automatically set to zero. In the present study and after tested different values we finally fixed the thresholds at 1% of the maximum values of these magnitudes [29]. Bicoherence values are roughly unity in the cases of constant phase, CP, (see Fig. 2c and 2f) and quadratic phase coupling, QPC (see, for instance, Fig. 2a and 2d). When a partial quadratic phase coupling, PQPC, is detected, the bicoherence values are between 0 and 1. The resultant values contain two important contributions, the first one corresponds to constant phase and the second one corresponds to pure quadratic phase coupling (see, for instance, Fig. 2b and 2e). Consequently, the percentage of partial coupling calculated from the biphase histograms could also be used to correct the value of the bicoherence.

The discrete trispectrum also was calculated as an average of the quadruple products of Fourier Transform over K segments:

$$\hat{T}_{4x}(f_1, f_2, f_3) = E[X(f_1)X(f_2)X(f_3)X^*(f_1 + f_2 + f_3)] \tag{5}$$

Hence the magnitude and triphase for the segment k, can simply be obtained as,

$$\left|T_{4x,k}(f_1, f_2, f_3)\right| = |X(f_1)X(f_2)X(f_3)X^*(f_1 + f_2 + f_3)| \tag{6}$$

$$\angle \mathrm{T}_{4x,k}(f_1, f_2, f_3) = \theta(f_1) + \theta(f_2) + \theta(f_3) - \theta(f_1 + f_2 + f_3) \tag{7}$$

Trispectrum relates three independent frequencies (f_1, f_2, f_3) and it is sensitive to the coupling between them. The principal domain of the discrete trispectrum is composed of two regions, the first one is defined by positives values of frequencies ($f_1 \geq 0$, $f_2 \geq 0$, $f_3 \geq 0$), in which the fourth frequency is equal to the sum of the three frequencies ($f_1 + f_2 + f_3 = f_4$). The second region, is defined by ($f_1 \geq 0$, $f_2 \geq 0$, $f_3 \leq 0$), and now, the frequency coupling results in a contribution at another frequency f_4 equal to $f_1 + f_2 - f_3$. If in both regions the triphase is zero or also ±π rad, as we argued before, there is Cubic Phase Coupling, CPC, phenomenon. Cubic phase coupling gives evidence of cubic nonlinearities in the mechanical system under study. As in the previous section, the triphase histogram technique is applied in order to check when cubic phase coupling conditions in frequency and phase are accomplished.

As it has been discussed before, to ensure statistical confidence the maximum segment size to compute the FT should be the $(r-1)^{th}$ root of the total length of the data when handling the r^{th} order spectrum [26, 32]. In the present trispectrum calculations, using 2048 points for the FT calculations, we need or a shortest FT segment or to increase the length of data under consideration. The first alternative implies a poor resolution in the calculations while that the second one implies a consideration of huge signals, around 8.6×10^9 data points, with the subsequent obvious problems of stationarity -not to mention that the duration of one real experiment do not allows the consideration of variable data lengths-. In order to solve the problem and to reduce as much as possible the spectral bias errors maintaining a segment size of 2048 points over 14000 windowed segments, the literature [32] suggests applying a special pre-whitening technique. In short, this technique simply filters the data in the time domain before the trispectrum is calculated. However, the linear filter used must be specially designed with a frequency response obtained as the square root of the inverse of the spectrum of the signal. So, to ensure statistical confidence, the present work adopted this pre-whitening technique using a spectral estimate based on 32767 points per segment and filtering all the signals before to calculate the trispectrum function.

Finally the trispectrum normalization -tricoherence function- has also been evaluated here using a Kim and Powers type of normalization [33],

$$\widehat{\mathrm{tric}}^2_{4x}(f_1,f_2,f_3) = \frac{\left|\hat{\mathrm{T}}_{4x}(f_1,f_2,f_3)\right|^2}{E[|X(f_1)X(f_2)X(f_3)|^2]\ \ \mathrm{E}[|\mathrm{X}(f_1+f_2+f_3)|^2]} \tag{8}$$

Also, as in the bicoherence case, low denominator magnitudes, can produce anomalous tricoherence peaks. For obviate this problem, we applied the same threshold methodology introduced in previous calculation of the bicoherence function.

3. Results

Despite the present work involved the analysis of many signals we mainly concentrate this report on four of them, corresponding to the maximum and minimum values of shaking amplitudes for two different frequencies. The first one -thereafter IVIDIL1- corresponds to 2.8 Hz of frequency and an amplitude of 31 mm (10/20/2009), the second one -called IVIDIL2- coincides with the frequency of IVIDIL1, but in this case has an amplitude of 15 mm (12/15/2009). The third signal -IVIDIL3- has a frequency of 2 Hz and its amplitude is 62 mm (12/09/2009). Finally, the fourth one -IVIDIL4- has the same frequency of IVIDIL3 although its amplitude is 31 mm (12/17/2009). In all cases we present plots of the entire signals analyzed (only X_A acceleration). As mentioned before, we have demeaned all raw signals treated, except the ones reported in Fig. 3 and Table 1 because we consider illustrative enough to highlight their global characteristics.

Fig. 3 shows the ten second interval average where it can be seen that the mean value is roughly the same in all cases. It is interesting to observe the presence of a disturbance in 'c)' signal around the 15h of the experiment, but this has been analyzed and does not produce any alteration in the results at all. Additional quantitative information is presented in Table 1. We can see that the medians do not coincide with the means indicating that the corresponding distributions are slightly skewed. Also it can be noted that the percentage of outliers is very low but there is a slight tendency to increase if the shaker amplitude increases (IVIDIL1 and IVIDIL3 cases). Finally, the interquartile range, IQR [36], indicates that equal shaker amplitude means similar values of IQR (IVIDIL1 and IVIDIL4). The highest IQR value, equivalently the highest data dispersion, is associated with the maximum shaker amplitude.

The histograms are shown in Fig. 4. All cases are multimodal, that is to say, nonGaussian. This fact is also found in all X_A acceleration components analyzed, despite they are not displayed here. The shaker breaks the Gaussianity only in one direction, but not in the other two (Y_A and Z_A).

The power spectral densities of the four X_A components are displayed in Fig. 5. The four periodograms indicate that the spectral response is always governed by the shaking frequency and its harmonics, but in all cases, the third harmonic shows a higher intensity than the fundamental one. This amazing situation has also been reported by Patel et al. [37] studying angular misaligned coupled rotors. Table 2 quantifies the intensities of the principal frequencies appearing. Clearly, for signals with the same shaking frequency, the intensity of the harmonics is a function of the shaking amplitude. Highest intensities mean maximum amplitudes. All these considerations are very interesting in order to understand and characterize the fluid behavior in thermodiffusion experiments as the SODI-IVIDIL one [38].

Fig. 6 presents the RMS acceleration versus one-third octave frequency bands only for the representative signals IVIDIL1, IVIDIL2, IVIDIL3 and IVIDIL4. Thick line, the ISS vibratory limit requirements allowed, indicates if the Columbus module really works in a microgravity mode. In the four cases the harmonic $3f_0$ exceeds the limits, however the fundamental frequency, f_0, pass only in "a)", "b)" and "c)" figures. Also, in the 2Hz signals we can see that the $5f_0$ harmonic has more intensity than the 2.8Hz signals, but this harmonic does not go beyond the requirements.

To study the kind of nonlinearity present in the experiments, the third-order spectrum is calculated. Fig. 7 and 8 show the bispectrum of the four signals. Notice that, as it has been mentioned before, both plots show redundant information in two symmetric regions separated by a symmetry axis which coincides with the diagonal of the first quadrant. In the case of IVIDIL1 and IVIDIL2 (f_0 = 2.8 Hz), the maximum bispectrum peak is located always in the same point (8.4, 8.4). For IVIDIL3 and IVIDIL4 (f_0 = 2 Hz) the maximum value changes depending on the amplitude of the harmonic oscillation, that is to say, for

a low value of amplitude the maximum bispectrum peaks are associated to the (6, 6) and (8, 6) couples while at highest amplitude the maximum bispectrum values are associated to the (6, 4) and (10, 6) pairs. As explained above, the peaks appearing in the bispectrum can be related to different behaviors clarified by the biphase histograms: constant phase (CP), partial quadratic phase coupling (PQPC) and quadratic phase coupling (CPC). Table 3 synthesizes all these aspects for the principal bispectrum peaks as a function of the different amplitudes of the movement. The first line (in parenthesis) presents the corresponding biphase situation -QPC, PQPC or CP- or the percentage of coupling for PQPC cases. The second line, in bold, shows the bicoherence values only in the cases of QPC and PQPC. Mention that, in the case of PQPC behavior, the bicoherence magnitude is due to both QPC and CP contributions -see, for instance, cases "b)" and "e)" of Fig. 2-, thus, the bicoherence values must be corrected taking into account the percentage of PQPC calculated. These last results are presented in brackets. Finally, it is interesting to pay special attention on the couples that could be related with an explanation of the higher intensities of the third harmonics 8.4 and 6 Hz respectively. The couple (5.6, 2.8) deserves a special attention because adding both frequencies the third harmonic (8.4 Hz) is obtained but, from Table 3, it presents a partial QPC behavior only for amplitudes 15 and 31 mm. A similar, but even worst, scenario is observed for IVIDIL3 and IVIDIL4 (f_0 = 2Hz). Thus, a quadratic nonlinear contribution seems to be not relevant enough to explain the strange energy distribution reported previously.

To go further, the trispectrum function was computed and displayed here using spheres with radii proportional to the root mean square of the trispectrum magnitude centered at the corresponding triplets. As before, the triphase of the main triplets has been investigated, and zero or $\pm\pi$ rad associated here to a CPC behavior. In addition, a constant triphase value, different to zero or $\pm\pi$ rad, sometimes appeared. As an example, Fig. 9 shows the trispectrum functions for IVIDIL1 and IVIDIL3. The biggest spheres are centered in (8.4, 8.4, -8.4) and (6, 6, -6) respectively. In a complementary way, Fig. 10 shows the triphase histograms associated with the above-mentioned values. It can be seen that the triphase distribution presents a very low dispersion around zero and consequently a cubic phase coupling could be associated to both mentioned frequency triplets. Table 4 summarizes all the results obtained for the main peaks that appear in the trispectrum for all the analyzed signals, included the intermediate ones. This table also presents, in bold, the tricoherence values. The maximum value of the trispectrum is always located at the above-mentioned points (8.4, 8.4, -8.4) and (6, 6, -6) for both shaking frequencies, 2.8 and 2 Hz and independently of the amplitude of the signals. CPC behavior has also been found at other points as (8.4, 2.8, -2.8) and (6, 2, -2). Taking into account all these last results, the higher power spectral intensities of the third harmonic could be explained. Additionally the high values of $5f_0$ frequency can be produced by CPC at the coupled frequencies (14, 8.4, -8.4) and (10, 6, -6). The tricoherence value associated to the peaks with CPC is, in all cases, around 1. Thus, based on this last set of results, it can be concluded that cubic symmetric nonlinearities are mainly responsible of the strange energy exchange detected. Moreover, taking into account the literature [14], it can be said that this anomalous behavior is probably due to a misalignment of the rotor axis of the motor located in the shaker.

4. Conclusions

Second and higher order spectral techniques have successfully been applied here to solve the problems proposed all along the present investigation concerning the SODI-IVIDIL experiments in the ISS. In effect, power spectral results on SAMS accelerometric signals have detected that, regardless of the working frequency, the third harmonic have higher intensities than the fundamental one. This amazing result indicates that the mechanical unit which generates the translational harmonic vibrations during the different IVIDIL runs acted as a nonlinear system distributing the energy in an anomalous way. This behavior is due to a malfunction of the device probably caused by a misalignment of the rotor axis. The nonlinear nature of internal motor interactions could generate complex dynamics that quickly redirects the energy in a nonlinear way, as in all the present cases. The use of third and fourth order spectral analyses allows us finally to identify the kind of these nonlinearities. In effect, although the bispectrum function shows different peaks indicating the existence of a coupling in frequency, the biphase histograms discards the couples that, even frequency coupled, do not present QPC phenomenon either. In general, we found that no relevant QPC behavior exists. On the other side, the trispectrum function detects that a wide cubic phase coupling phenomenon exist in all the signals. This mechanism of energy exchange is, thus, the responsible of the high power spectral intensities associated with the third harmonic and even with the fifth one.

As a global conclusion of the present work, mention that all these considerations are important not only in generic research of aerospace engineering but also in space sciences in order to help space researchers to characterize even more globally their particular experiments. In effect, the proposed technique is an efficient tool for detecting fingerprints of bad mechanical coupling or the health of the shaker mechanics and its degradation. Besides, the researchers should pay attention to the valuable dynamic information contained in the accelerometric results in order to better contextualize the experiment in the subsequent theoretical models used to study it. These adjustments are even more important if the system is a liquid one and interacts with external vibrations which could in turn influence its dynamic behavior.

Acknowledgments

The content of the present work is part of our participation in the HSF-US/2010-041 and HSF-US/2010-042 ESA projects.

References

[1] V. Shevtsova, A. Mialdun, D. Melinkov, I. Ryzhkov, Y. Gaponenko, Z. Saghir, Y. Lyubimova, J.C. Legros, The IVIDIL experiment on-board the ISS: Thermodiffusion in the presence of controlled vibrations, C. R. Mec., 339 (2011), pp. 310-317. DOI: 10.1016/j.crme.2011.03.007

[2] A. Rodríguez, J. Rodríguez, A. Laverón-Simavilla, V. Lapuerta, Results and experiences from the SODI-IVIDIL experiment on the ISS, Proceedings of the sixty-first International Astronautical Congress (IAC), Czech Republic, 2010, pp. 10283-10287.

[3] K. McPherson, J. Keller, E. Kelly, K. Hrovat, The NASA Glenn research center's acceleration measurement and analysis projects support for the international space station (ISS), 16th CASI astronautics conference, ASTRO 2012, Quebec City, 2012.

[4] A. Rivola, P.R. White, Detecting system nonlinearities by means of higher order statistics, Bulletin S.F.M. Revue Française de Mécanique, Vol. 2, 1999, pp. 129-136.

[5] G. Kerschen, K. Worden, A.F. Vakakis, J.C. Golinval, Past, present and future of nonlinear system identification in structural dynamics, Mech. Syst. Signal Pr., 20 (2006), pp. 505-592. DOI:10.1016/j.ymssp.2005.04.008

[6] D. Hickey, K. Worden, M.F. Platten, J.R. Wright, J.E. Cooper, Higher-order spectra for identification of nonlinear modal coupling, Mech. Syst. Signal Pr., 23 (2009) pp. 1037-1061. DOI:10.1016/j.ymssp.2008.10.008

[7] A.J. Hillis, S.A. Neild, B.W. Drinkwater, P.D. Wilcox, Global crack detection using bispectral analysis, Proceedings of the Royal Society A, 462 (2006), pp. 1515-1530. DOI:10.1098/rspa.2005.1620

[8] J.K. Sinha, Bispectrum of a rotating shaft with a breathing crack, Adv. Vib. Eng., 7(4) (2008), pp. 301-310. DOI:10.1007/978-94-007-0020-8_43

[9] M. Jasinski, S. Radkowski, Use of the higher spectra in the low-amplitude fatigue testing, Mech. Syst. Signal Pr., 25 (2011) pp. 704-716. DOI:10.1016/j.ymssp.2010.06.001

[10] G. Dalpiaz, A. Rivola, R. Rubini, Effectiveness and sensitivity of vibration processing techniques for local fault detection in gears, Mech. Syst. Signal Pr., 14 (2000), pp. 387–412. DOI:10.1006/mssp.1999.1294

[11] H. Li, Order bispectrum for bearing fault monitoring and diagnosis under run-up condition, J. Comput., 6 (2011), pp. 1994-2000. DOI:10.4304/jcp.6.9.1994-2000

[12] K. Elbhbah, J.K. Sinha, Bispectrum for fault diagnosis in rotating machines, Proceedings of the seventeenth International Congress on Sound and Vibration, Cairo, 2010, pp. 1290-1297.

[13] L. Jiang, Y. Liu, X. Li, S. Tang, Using bispectral distribution as a feature for rotating machinery fault diagnosis, Measurement, Vol. 44, 2011, pp. 1284-1292. DOI:10.1016/j.measurement.2011.03.024

[14] J.K. Sinha, K. Elbhbah, A future possibility of vibration based condition monitoring of rotating machines, Mech. Syst. Signal Pr., 34 (2013), pp. 231-240. DOI:10.1016/j.ymssp.2012.07.001

[15] F. Gu, Y. Shao, N. Hu, A. Naid, A.D. Ball, Electrical motor current signal analysis using a modified bispectrum for fault diagnosis of downstream mechanical equipment, Mech. Syst. Signal Pr., 25 (2011), pp. 360-372. DOI:10.1016/j.ymssp.2010.07.004

[16] F.E. Hernández, O. Caveda, The application of bispectrum on diagnosis of rolling elements bearings: a theoretical approach, Mech. Syst. Signal Pr., 22 (2008), pp. 588-596. DOI:10.1016/j.ymssp.2007.09.003

[17] K. Fitzpatrick, M. Grygier, M. Laible, S. Sugavanam, International Space Station Modal Correlation Analysis, Topics in Model Validation and Uncertainty Quantification: Conference proceedings of the Society for Experimental Mechanics Series 41, edited by T. Simmermacher et al., Vol. 5, 2013, pp. 221-242. DOI:10.1007/978-1-4614-6564-5_22

[18] M. Laible, K. Fitzpatrick, M. Grygier, International Space Station 2A Array Modal Analysis. G. Kerschen et al. (Eds.), Topics in Nonlinear Dynamics: Proceedings of the 31st IMAC, A Conference on Structural Dynamics. Conference proceedings of the Society for Experimental Mechanics Series 35, Vol. 1, Los Angeles, 2013, pp. 1-14. DOI:10.1007/978-1-4614-6570-6 1

[19] N. Sáez, X. Ruiz, J. Pallarés, V. Shevtsova, On the accuracy of the interdiffusion coefficient measurements of high temperature binary mixtures under ISS conditions, C. R. Mec., 341(4–5) (2013), pp. 405-416. DOI:10.1016/j.crme.2013.02.007

[20] N. Sáez, X. Ruiz, Jna. Gavaldà, J. Pallarés, V. Shevtsova, Comparative ISS accelerometric analyses, Acta Astronaut., 94(2) (2014), pp. 681-689. DOI:10.1016/j.actaastro.2013.09.005

[21] A. Rivola, P.R. White, Use of higher order spectra in condition monitoring: simulation and experiments, Proceedings of ASME Design Engineering Technical Conferences, DETC99/VIB-8332, Las Vegas, Nevada, 1999, pp. 12-16.

[22] J.M. Nichols, P. Marzocca, A. Milanese, On the use of the auto-bispectral density for detecting quadratic nonlinearity in structural systems, J. Sound Vib., 312 (2008), pp. 726-735. DOI:10.1016/j.jsv.2007.11.032

[23] C.R.P. Courtney, S.A. Neild, P.D. Wilcox, B.W. Drinkwater, Application of the bispectrum for detection of small nonlinearities excited sinusoidally, J. Sound Vib., 329 (2010), pp. 4279-4203. DOI:10.1016/j.jsv.2010.04.031

[24] K. Jules, K. McPherson, K. Hrovat, E. Kelly, Initial characterization of the microgravity environment of the international space station: increments 2 through 4, Acta Astronaut., 55(10) (2004), pp. 855-887. DOI:10.1016/j.actaastro.2004.04.008

[25] M.J.B. Rogers, K. Hrovat, K. McPherson, M.E. Moskowitz, T. Reckart, Accelerometer data analysis and presentation techniques, NASA center, Ohio aerospace institute, Cleveland, Ohio, 1997.
[26] A. Rivola, Applications of higher order spectra to the machine condition monitoring, Publication in Dipartimento di ingegneria delle costruzioni meccaniche, nucleari, aeronautiche e di metallurgia, Vol. 107, DIEM, University of Bologna, 2000.
[27] V. Chandran, S. Elgar, A general procedure for the derivation of principal domains of higher-order spectra, IEE transitions on signal processing, Vol. 42, No. 1, 1994, pp. 229-233. DOI:10.1109/78.258147
[28] D. Wong, D.A. Clifton, L. Tarassenko, An introduction to the bispectrum for EEG analysis. C.J. James et al. (Eds), Proceedings of the 5th UK & Republic of Ireland postgraduate conference in biomedical engineering and medical physics, PGBIOMED09, IEEE UKRI EMB Student Club, Oxford, U.K., 2009, pp.61-62.
[29] N. Jaksic, M. Boltezar, I. Simonovski, A. Kuhelj, Dynamical behavior of the planar nonlinear mechanical system - Part I: theoretical modeling, J. Sound Vib., 226(5) (1999), pp. 923-940. DOI:10.1006/jsvi.1999.2240
[30] J.W.A. Fackrell, P.R. White, J.K. Hammond, R.J. Pinnington, A.T. Parsons, The interpretation of the bispectra of vibration signals. I.- Theory, Mech. Syst. Signal Pr., 9 (1995), pp. 257-266. DOI:10.1006/mssp.1995.0021
[31] J.W.A. Fackrell, P.R. White, J.K. Hammond, R.J. Pinnington, A.T. Parsons, The interpretation of the bispectra of vibration signals. II.- Experimental results and applications, Mech. Syst. Signal Pr., 9 (1995), pp. 267-274. DOI:10.1006/mssp.1994.0022
[32] W. B. Collis, P.R. White, J.K. Hammond, Higher-order spectra: the bispectrum and trispectrum, Mech. Syst. Signal Pr., 12(3) (1998), pp. 375-394. DOI:10.1006/mssp.1997.0145
[33] Y.C. Kim, E.J. Powers, Digital bispectral analysis and its applications to nonlinear wave interactions, IEEE transactions on plasma science, 7(2) (1979), pp. 120-131. DOI:10.1109/TPS.1979.4317207
[34] M. Boltezar, N. Jaksic, I. Simonovski, A. Kuhelj, Dynamical behaviour of the planar nonlinear mechanical system - Part II: experiment, J. Sound Vib., 226(5) (1999), pp. 941-953. DOI:10.1006/jsvi.1999.2245
[35] S. Elgar, G. Sebert, Statistics of bicoherence and biphase", J. geophys. res., 94(8) (1989), pp. 993-998. DOI:10.1029/JC094iC08p10993
[36] R. McGill, J.W. Tukey, W.A. Larsen, Variation of Boxplots, The American Statistician Publications, Vol. 32, No. 1, 1978, pp. 12-16.
[37] T. H. Patel, A.K. Darpe, Vibration response of misaligned rotors, J. Sound Vib., 325 (2009), pp. 609-628. DOI:10.1016/j.jsv.2009.03.024
[38] V. Shevtsova, Y. Lyubimova, Z. Saghir, D. Melinkov, Y. Gaponenko, V. Sechenyh, J.C. Legros, A. Mialdun, IVIDIL: on-board g-jitters and diffusion controlled phenomena, J. Phys., Conference Series, 27 (2011), 012031. DOI: 10.1088/1742-6596/327/1/012031

Fig.1: Phase of the Fourier Transform.

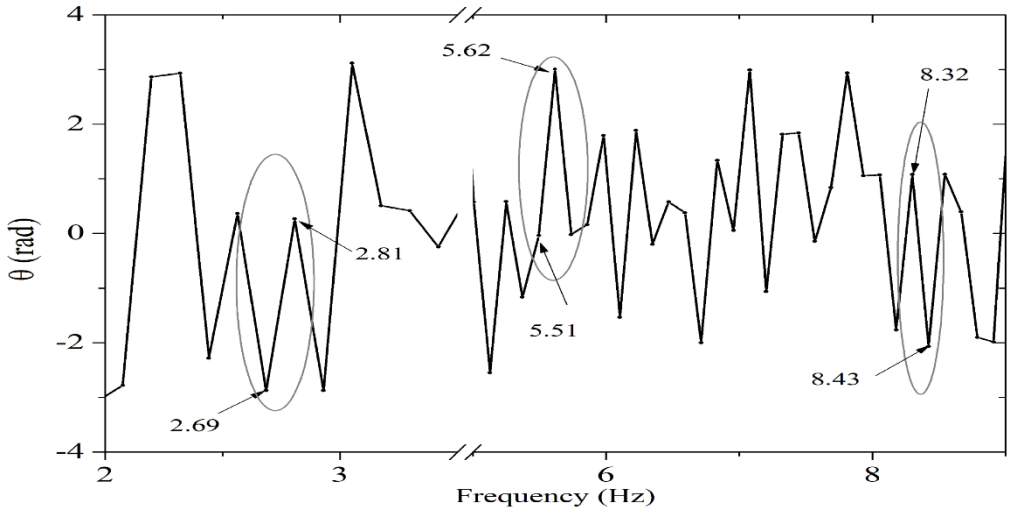

Fig.2: Typical biphase histograms. a) QPC, b) PQPC, c) CP, d) QPC, e) PQPC and f) CP.

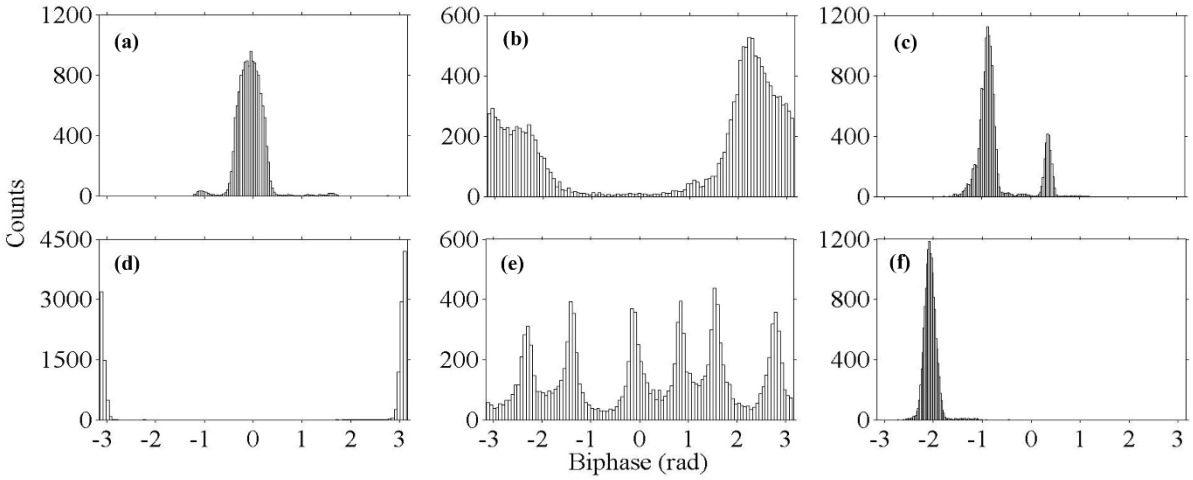

Fig.3: 10s interval average of X_A axis acceleration. a) IVIDIL1, b) IVIDIL2, c) IVIDIL3 and d) IVIDIL4.

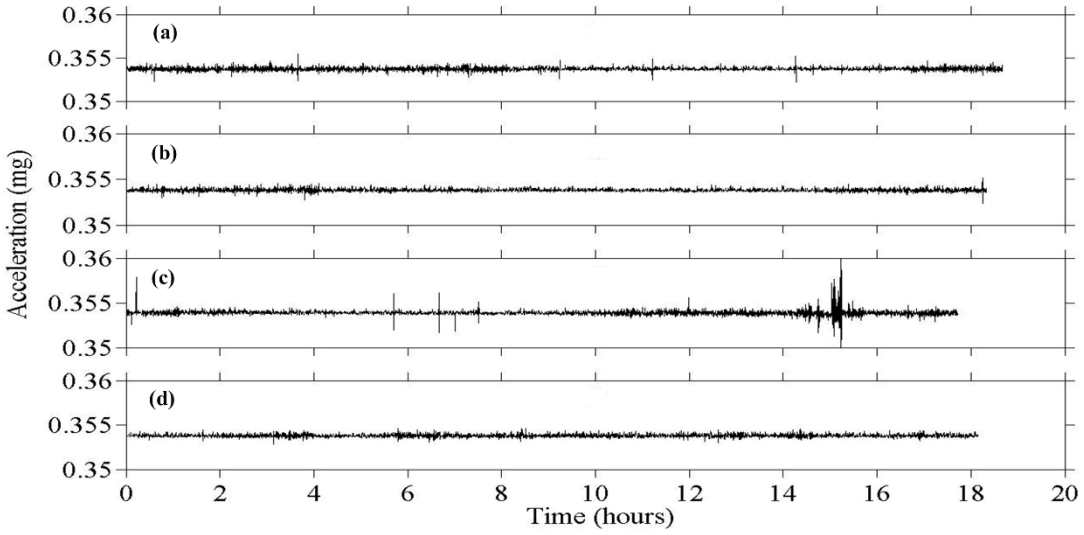

Fig.4: Histograms of X_A. a) IVIDIL1, b) IVIDIL2, c) IVIDIL3 and d) IVIDIL4.

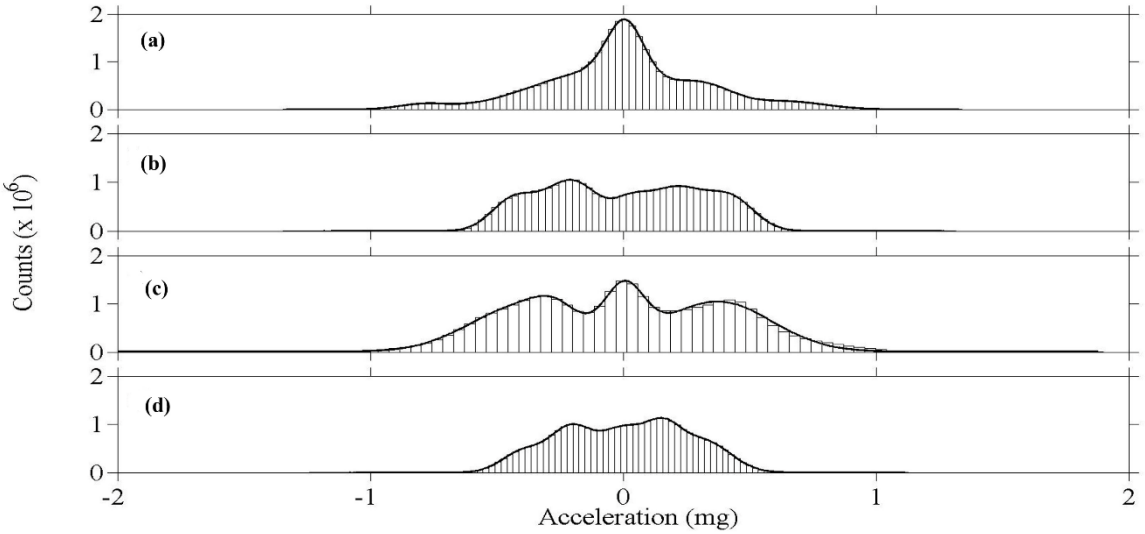

Fig.5: Power Spectral Density of X_A acceleration. a) IVIDIL1, b) IVIDIL2, c) IVIDIL3 and d) IVIDIL4

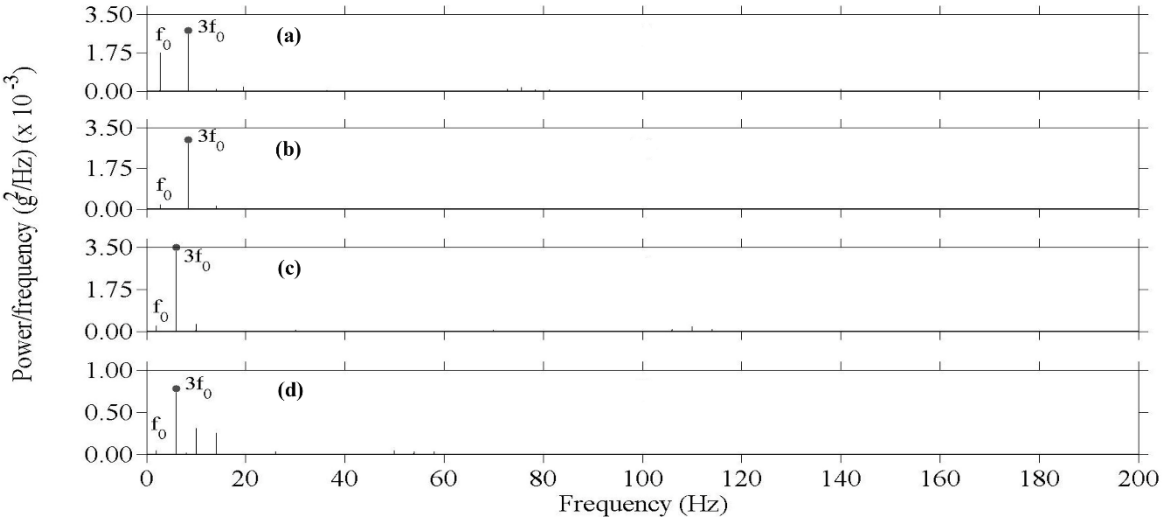

Fig.6: RMS acceleration. a) IVIDIL1, b) IVIDIL2, c) IVIDIL3 and d) IVIDIL4.

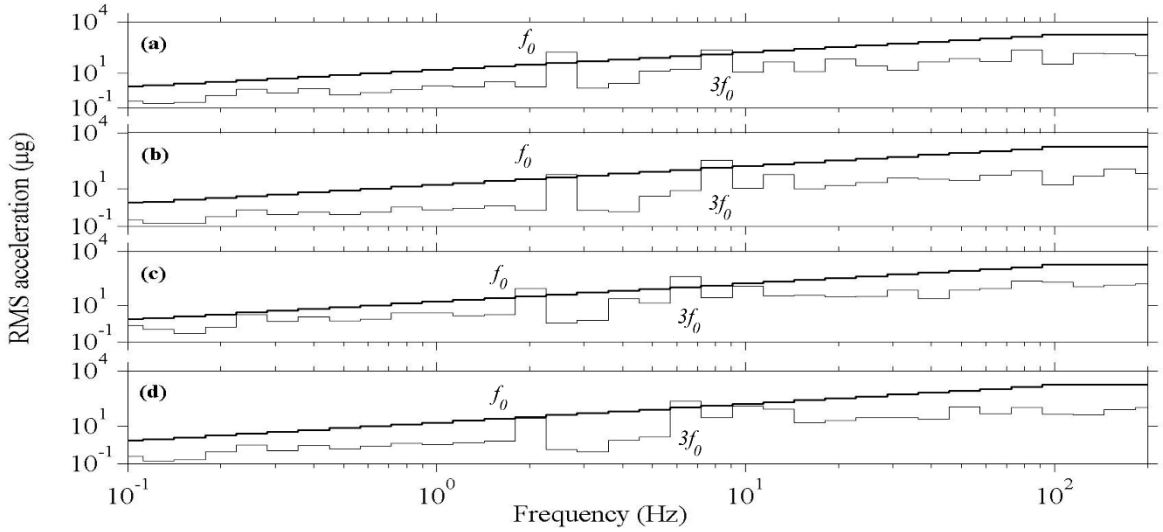

Fig.7: Bispectrum. a) IVIDIL1 and b) IVIDIL2.

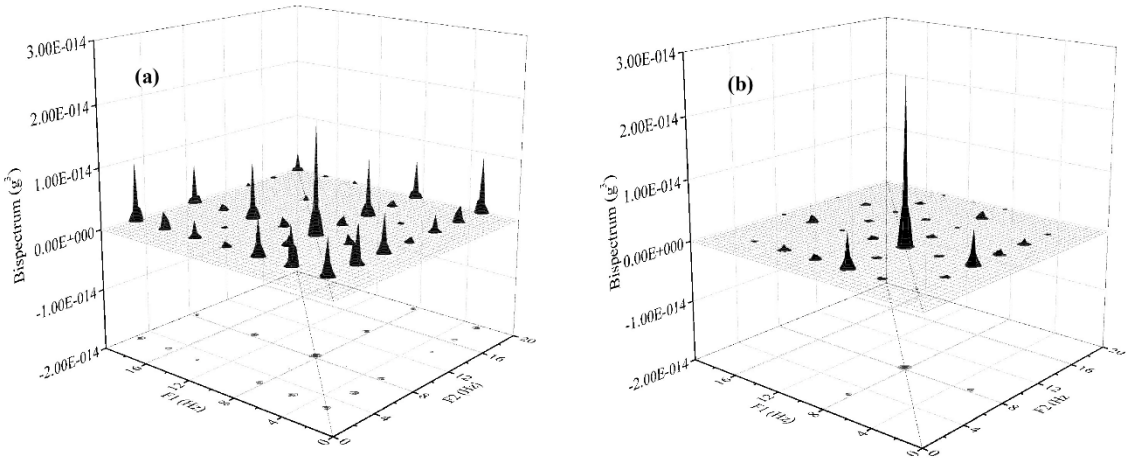

Fig.8: Bispectrum. a) IVIDIL3 and b) IVIDIL4.

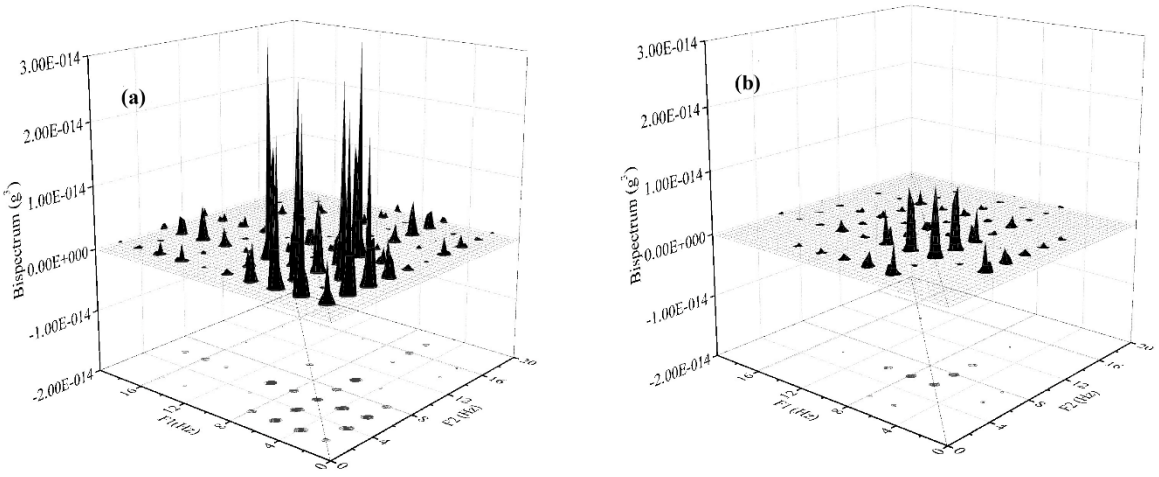

Fig.9: Trispectrum. a) IVIDIL1 and b) IVIDIL3.

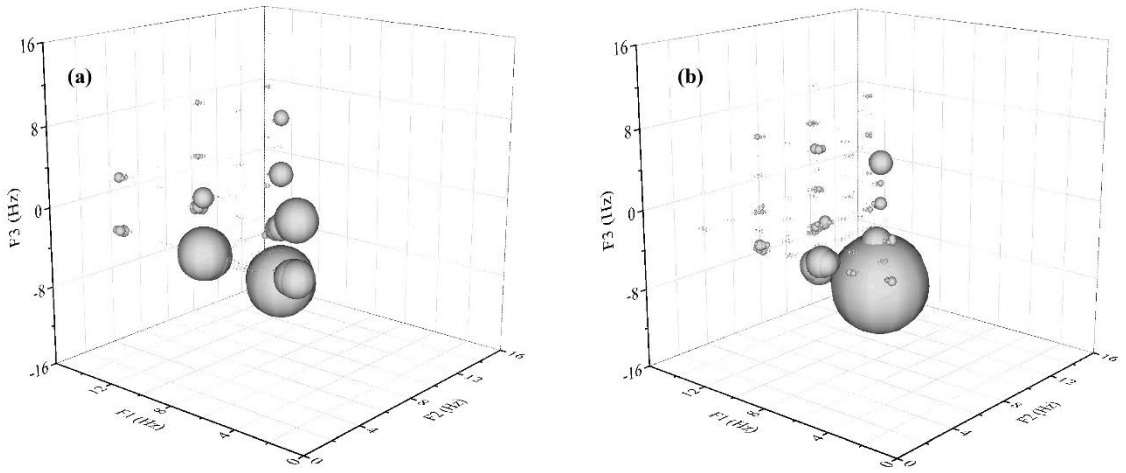

Fig.10: Triphase. a) IVIDIL1 (8.4, 8.4, -8.4) and b) IVIDIL3 (6, 6, -6).